nature research

https://doi.org/10.1038/s41567-020-01120-z

Supplementary information

Floquet prethermalization in dipolar spin chains

In the format provided by the authors and unedited

Supplementary information for observation of Floquet prethermalization in dipolar spin chains

Pai Peng,[1,*] Chao Yin,[2,†] Xiaoyang Huang,[2] Chandrasekhar Ramanathan,[3] and Paola Cappellaro[4,2,‡]

[1] *Department of Electrical Engineering and Computer Science, Massachusetts Institute of Technology, Cambridge, MA 02139*

[2] *Research Laboratory of Electronics, Massachusetts Institute of Technology, Cambridge, Massachusetts 02139, USA*

[3] *Department of Physics and Astronomy, Dartmouth College, Hanover, NH 03755, USA*

[4] *Department of Nuclear Science and Engineering, Massachusetts Institute of Technology, Cambridge, MA 02139*

(Dated: October 1, 2020)

I. EXPERIMENTAL SYSTEM, CONTROL AND DATA ANALYSIS

A. Experimental System

The system used in the experiment was a single crystal of fluorapatite (FAp). Fluorapatite is a hexagonal mineral with space group $P6_3/m$, with the ^{19}F spin-1/2 nuclei forming linear chains along the c-axis. Each fluorine spin in the chain is surrounded by three ^{31}P spin-1/2 nuclei. We used a natural crystal, from which we cut a sample of approximate dimensions 3 mm×3 mm×2 mm. The sample is placed at room temperature inside an NMR superconducting magnet producing a uniform $B = 7$ T field. The total Hamiltonian of the system is given by

$$H_{\rm tot} = \omega_F \sum_k S_z^k + \omega_P \sum_\kappa s_z^\kappa + H_F + H_P + H_{FP} \quad (1)$$

The first two terms represent the Zeeman interactions of the F(S) and P(s) spins, respectively, with frequencies $\omega_F = \gamma_F B \approx (2\pi)282.37$ MHz and $\omega_P = \gamma_P B = (2\pi)121.51$ MHz, where $\gamma_{F/P}$ are the gyromagnetic ratios. The other three terms represent the natural magnetic dipole-dipole interaction among the spins, given generally by

$$H_{\rm dip} = \sum_{j<k} \frac{\hbar\gamma_j\gamma_k}{|\vec{r}_{jk}|^3}\left[\vec{S}_j\cdot\vec{S}_k - \frac{3\vec{S}_j\cdot\vec{r}_{jk}\,\vec{S}_k\cdot\vec{r}_{jk}}{|\vec{r}_{jk}|^2}\right], \quad (2)$$

where $\vec{r}_{ij}$ is the vector between the ij spin pair. Because of the much larger Zeeman interaction, we can truncate the dipolar Hamiltonian to its energy-conserving part (secular Hamiltonian). We then obtain the homonuclear Hamiltonians

$$\begin{aligned} H_F &= \frac{1}{2}\sum_{j<k} J_{jk}^F(2S_z^jS_z^k - S_x^jS_x^k - S_y^jS_y^k) \\ H_P &= \frac{1}{2}\sum_{\lambda<\kappa} J_{\kappa\lambda}^P(2s_z^\lambda s_z^\kappa - s_x^\lambda s_x^\kappa - s_y^\lambda s_y^\kappa) \end{aligned} \quad (3)$$

and the heteronuclear interaction between the F and P spins,

$$H_{FP} = \sum_{k,\kappa} J_{k,\kappa}^{FP} S_z^k s_z^\kappa, \quad (4)$$

with $J_{jk} = \hbar\gamma_j\gamma_k\frac{1-3\cos(\theta_{jk})^2}{|\vec{r}_{jk}|^3}$, where θ_{jk} is the angle between the vector $\vec{r}_{jk}$ and the magnetic field z-axis. The maximum values of the couplings (for the closest spins) are given respectively by $J^F = -32.76$ krad s^{-1}, $J^P = 1.20$ krad s^{-1} and $J^{FP} = 6.12$ krad s^{-1}, estimated from the crystal structure. If the crystal's c-axis is aligned with the magnetic field, these will be the coupling strength. In experiments, We measure the coupling of nearest neighbor ^{19}F to be $J_0 = -29.7$ krad/s by fitting $\langle X(t)X\rangle$ under the double quantum Hamiltonian to the analytical form [1].

The dynamics of this complex many-body system can be mapped to a much simpler, quasi-1D system. First, we note that when the crystal is oriented with its c-axis parallel to the external magnetic field the coupling of fluorine spins to the closest off-chain fluorine spin is ≈ 40 times weaker, while in-chain, next-nearest neighbor couplings are 8 times weaker. Previous studies on these crystals have indeed observed dynamics consistent with spin chain models, and the system has been proposed as solid-state realizations of quantum wires [2–4]. This approximation of the experimental system to a 1D, short-range system, although not perfect has been shown to reliably describe experiments for relevant time-scales [5, 6]. The approximation breaks down at longer times, with a con-

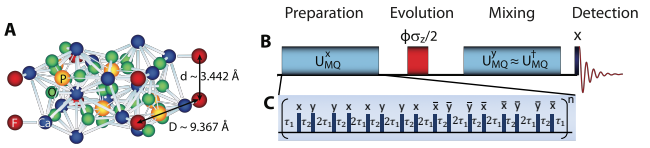

Fig. 1. **A** Fluorapatite crystal structure, showing the Fluorine and Phosphorus spins in the unit cell. **B** NMR scheme for the generation and detection of MQC. In the inset (**C**) an exemplary pulse sequence for the generation of the $H_{\rm dipy}$. Note that thanks to the ability of inverting the sign of the Hamiltonian, the scheme amounts to measuring out-of-time order correlations.

* paipeng@mit.edu
† P.P. and C.Y. contributed equally to this work.
‡ pcappell@mit.edu

vergence of various effects: long-range in-chain and cross-chain couplings, as well as pulse errors in the sequences used for Hamiltonian engineering. In addition, the system also undergoes spin relaxation, although on a much longer time-scale ($T_1 = 0.8$ s for our sample).

B. Error analysis

In experiments, we want to measure the correlation $\langle \delta\rho(t)\mathcal{O}\rangle$, where $\delta\rho(t) = U(t)\delta\rho(0)U(t)$ is the nontrivial part of the density matrix evolved under a pulse-control sequence for a time t. Instead of just performing a single measurement after the sequence, we continuously monitor the free evolution of $\delta\rho(t)$ under the natural Hamiltonian $H_{\rm dip}$, from t to $t + t_{\rm FID}$. The measured signal is called in NMR free induction decay (FID) and a typical FID trace is shown in Fig. 2). This signal trace allows us to extract not only the amplitude of the correlation (from the first data point) but also its uncertainty. We take the standard deviation of the last 20 data points in the FID as the uncertainty of the $\langle \delta\rho(t)\mathcal{O}\rangle$. This uncertainty is used with linear error propagation to obtain the error bars of all the quantities analyzed in the main text.

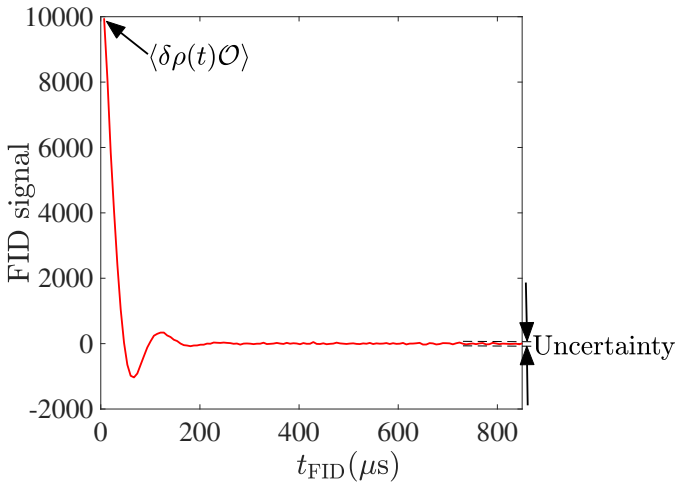

Fig. 2. An example of FID. 128 data points are taken in total. The first data point gives $\langle(\delta\rho(t)\mathcal{O}\rangle$ and the standard deviation of the last 20 points gives the uncertainty of $\langle(\delta\rho(t)\mathcal{O}\rangle$.

C. Hamiltonian Engineering

In the main text we focused on the Floquet heating (Trotter error) for a periodic alternating scheme, switching between two Hamiltonians. In order to avoid longer times and/or different numbers of control operations when changing the Trotter step (Floquet period), we engineered Hamiltonians of variable strengths. Then, the Hamiltonians themselves are obtained stroboscopically by applying periodic rf pulse trains to the natural dipolar Hamiltonian that describes the system, and are thus themselves Floquet Hamiltonians. Since we only varied the sequences, but not the Floquet period, errors in this step contribute to the background decay but not the Floquet heating described in the main text, as we investigate in methods.

We used Average Hamiltonian Theory (AHT) [7] as the basis for our Hamiltonian engineering method, to design the control sequences and determine the approximation errors. The dynamics is induced by the total Hamiltonian $H = H_{\rm dip} + H_{\rm rf}$, where $H_{\rm dip} = \frac{1}{2}\sum_{j<k} J_{jk}(2S_z^jS_z^k - S_x^jS_x^k - S_y^jS_y^k) + \sum_j h_jS_z^j$ is the system Hamiltonian, and $H_{\rm rf}(t)$ is the external Hamiltonian due to the rf-pulses. The density matrix ρ evolves under the total Hamiltonian according to $\dot\rho = -i[H,\rho]$. We study the dynamics into a convenient interaction frame, defined by $\rho' = {U_{\rm rf}}^\dagger \rho U_{\rm rf}$, where $U_{\rm rf}(t) = \mathcal{T}\exp[-i\int_0^t H_{\rm rf}(t')dt']$ and $\mathcal{T}$ is the time ordering operator. In this *toggling* frame, ρ' evolves according to $\dot\rho' = -i[H(t),\rho']$, where $H(t) = {U_{\rm rf}}^\dagger H_{\rm dip} U_{\rm rf}$. Since $U_{\rm rf}$ is periodic, $H(t)$ is also periodic with the same period τ, and gives rise to the Floquet Hamiltonian, H_F, as as $U(\tau) = \exp[-iH_F\tau]$. Note that if the pulse sequence satisfies the condition $U_{\rm rf}(\tau) = 1$, the dynamics of ρ and ρ' are identical when the system is viewed stroboscopically, i.e., at integer multiples of τ, where the toggling frame coincides with the (rotating) lab frame.

We devised control sequences to engineer a scale-down, rotated version of the dipolar Hamiltonian [8, 9]. We usually look for control sequences that would engineer the desired Hamiltonian up to second order in the Magnus-Floquet expansion. Then, to engineer the interaction D_y, we use a 16-pulse sequence. The basic building block is given by a 4-pulse sequence [10, 11] originally developed to study MQC. We denote a generic 4-pulse sequence as $P(\tau_1,\mathbf{n}_1,\tau_2,\mathbf{n}_2,\tau_3,\mathbf{n}_3,\tau_4,\mathbf{n}_4,\tau_5)$, where $\mathbf{n}_j$ represents the direction of the j-th $\pi/2$ pulse, and τ_j's the delays interleaving the pulses. In our experiments, the $\pi/2$ pulses have a width t_w of 1.02 μs. τ_j starts and/or ends at the midpoints of the pulses (see also Fig. 1). In this notation, our forward 16-pulse sequence can be expressed as

$$P(\tau_1,\mathbf{x},\tau_2,\mathbf{y},2\tau_1,\mathbf{y},\tau_2,\mathbf{x},\tau_1)P(\tau_1,\mathbf{x},\tau_2,\mathbf{y},2\tau_1,\mathbf{y},\tau_2,\mathbf{x},\tau_1)P(\tau_1,\overline{\mathbf{x}},\tau_2,\overline{\mathbf{y}},2\tau_1,\overline{\mathbf{y}},\tau_2,\overline{\mathbf{x}},\tau_1)P(\tau_1,\overline{\mathbf{x}},\tau_2,\overline{\mathbf{y}},2\tau_1,\overline{\mathbf{y}},\tau_2,\overline{\mathbf{x}},\tau_1)$$

and the backward sequence as

$$P(\tau_3,\mathbf{y},\tau_3,\mathbf{x},2\tau_4,\mathbf{x},\tau_3,\mathbf{y},\tau_3)P(\tau_3,\mathbf{y},\tau_3,\mathbf{x},2\tau_4,\mathbf{x},\tau_3,\mathbf{y},\tau_3)P(\tau_3,\overline{\mathbf{y}},\tau_3,\overline{\mathbf{x}},2\tau_4,\overline{\mathbf{x}},\tau_3,\overline{\mathbf{y}},\tau_3)P(\tau_3,\overline{\mathbf{y}},\tau_3,\overline{\mathbf{x}},2\tau_4,\overline{\mathbf{x}},\tau_3,\overline{\mathbf{y}},\tau_3)$$

where $\{\overline{\mathbf{x}}, \overline{\mathbf{y}}\} \equiv \{-\mathbf{x}, -\mathbf{y}\}$. The delays are given by

$$\tau_1 = \tau_0(1-u), \quad \tau_2 = \tau_0(1+2u),$$
$$\tau_3 = \tau_0(1+u), \quad \tau_4 = \tau_0(1-2u),$$

where τ_0 is 5 μs in this paper. The cycle time τ, defined as the total time of the sequence, is given by $\tau = 24\tau_0$. u is a dimensionless adjustable parameter, and is restricted such that none of the inter-pulse spacings becomes negative. To the zeroth order Magnus expansion, the above sequence realizes Hamiltonian uJ_0D_y and $uJ_0 = J$.

A uniform transverse field can be introduced in $H^{(0)}$ by phase-shifting the entire pulse sequence. Consider rotating the n-th cycle of the pulse sequence by $(n-1)\phi$ around the $\mathbf{z}$ axis, which can be accomplished by phase shifting all the pulse directions $\mathbf{n}_j$ in the n-th cycle by $(n-1)\phi$. The evolution operator for each cycle is given by

$$\begin{aligned} U_1 &= e^{-iJD_y\tau}, \\ U_2 &= e^{i\phi Z}e^{-iJD_y\tau}e^{-i\phi Z}, \\ U_3 &= e^{2i\phi Z}e^{-iJD_y\tau}e^{-2i\phi Z}, \\ &\cdots \\ U_n &= e^{i(n-1)\phi Z}e^{-iJD_y\tau}e^{-i(n-1)\phi Z} \end{aligned}$$

where $Z = \sum_j S_z^j$. The total evolution operator over n cycles is given by the product:

$$\begin{aligned} U(n\tau) &= U_nU_{n-1}\cdots U_3U_2U_1 \\ &= e^{in\phi Z}\left[e^{-i\phi Z}e^{-iJD_y\tau}\right]^n \end{aligned}$$

where the Floquet sequence is then given by $H_1 = JD_y \quad H_2 = hZ$, with $h = \phi/\tau$. The rotation approach also generates an extra term $e^{in\phi Z}$, this term can be canceled in MQC experiments by rotating the observable by $n\phi$.

We note that our methods can be applied more broadly to engineer desired Hamiltonians H_{des} using only collective rotations of the spins applied to the naturally occurring Hamiltonian, H_{nat}. The engineered Hamiltonian is obtained by piece-wise constant evolution under-rotated versions of the natural Hamiltonian under the condition $\sum_k R_k H_{nat} R_k^\dagger = H_{des}$, where R_k are collective rotations of all the spins, which achieves the desired operator to first order in a Magnus expansion. Symmetrization of the sequence can further cancel out the lowest order correction. Using only collective pulses limits which Hamiltonians can be engineered, due to symmetries of the natural Hamiltonian and the action of collective operators. For typical two-body interactions of spin-1/2, an efficient tool to predict which Hamiltonians are accessible is to use spherical tensors [12].

II. FIT OF HEATING RATES

In the main text we fit the autocorrelation decay rates by an exponential function $\langle \mathcal{O}(n)\mathcal{O}\rangle \propto \exp(-\gamma n)$ using data within range $n \in [20, 64]$ to exclude transient effects. Since neither the specific form of the decay function nor the end of the transient dynamics is known exactly, in this section we present the decay rates obtained when varying the fitting range and the fitting function and show that these do not qualitatively change their behavior and thus our conclusions. Figure 3 depicts the decay rates obtained from an exponential fitting of the data over different ranges. Fitting a smaller range starting at later time results in a slightly smaller decay rate (with larger uncertainty), but the exponential trend is unchanged. In Fig. 4 we compared fitting to an exponential and to a stretched exponential function, $\langle \mathcal{O}(n)\mathcal{O}\rangle = \langle \mathcal{O}(0)\mathcal{O}\rangle \exp(-(t/\tau_K)^\alpha)$. We choose the stretched exponential because it is a good model for exponential decays under a distribution of decay rates. Here we plot the inverse of the mean relaxation time of

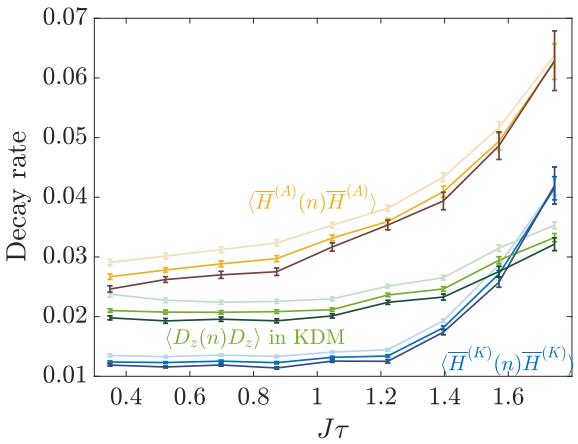

Fig. 3. Fitted decay rates for different fitting range: $n \in [10, 64]$ (light colors), $n \in [20, 64]$ (intermediate colors) and $n \in [30, 64]$ (dark colors).

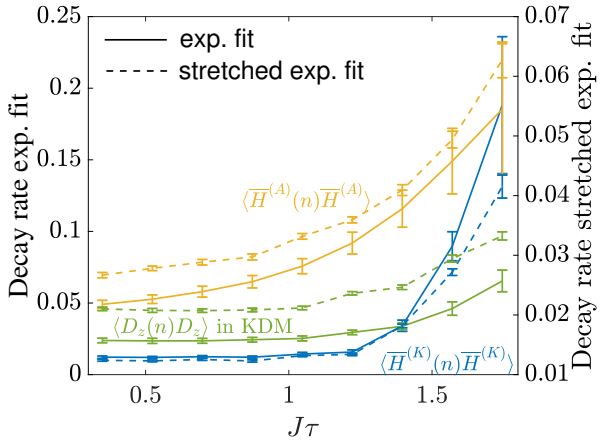

Fig. 4. Fitted decay rates using exponential fitting (solid curves, left axis) and stretched exponential fitting (dashed curves, right axis). Fitting range is $n \in [20, 64]$.

a stretched exponential function,

$$1/\gamma = \langle \tau_R \rangle = \frac{\tau_K}{\alpha} \Gamma \left(\frac{1}{\alpha} \right), \tag{5}$$

where Γ is the Gamma function. The decay rates from both fitting models are qualitatively the same.

[1] S. Doronin, I. Maksimov, and E. Fel'dman, JETP **91**, 597 (2000).
[2] P. Cappellaro, C. Ramanathan, and D. G. Cory, Phys. Rev. Lett. **99**, 250506 (2007).
[3] P. Cappellaro, L. Viola, and C. Ramanathan, Phys. Rev. A **83**, 032304 (2011).
[4] C. Ramanathan, P. Cappellaro, L. Viola, and D. G. Cory, New J. Phys. **13**, 103015 (2011).
[5] E. Rufeil-Fiori, C. M. Sánchez, F. Y. Oliva, H. M. Pastawski, and P. R. Levstein, Phys. Rev. A **79**, 032324 (2009).
[6] W. Zhang, P. Cappellaro, N. Antler, B. Pepper, D. G. Cory, V. V. Dobrovitski, C. Ramanathan, and L. Viola, Phys. Rev. A **80**, 052323 (2009).
[7] U. Haeberlen and J. Waugh, Phys. Rev. **175**, 453 (1968).
[8] K. X. Wei, C. Ramanathan, and P. Cappellaro, Phys. Rev. Lett. **120**, 070501 (2018).
[9] K. X. Wei, P. Peng, O. Shtanko, I. Marvian, S. Lloyd, C. Ramanathan, and P. Cappellaro, Phys. Rev. Lett. **123**, 090605 (2019).
[10] G. Kaur and P. Cappellaro, New J. Phys. **14**, 083005 (2012).
[11] Y.-S. Yen and A. Pines, J. Chem. Phys. **78**, 3579 (1983).
[12] A. Ajoy and P. Cappellaro, Phys. Rev. Lett. **110**, 220503 (2013).